Ionization of atoms in parallel electric and magnetic fields: The role of classical phase space

W. Ihra, F. Mota-Furtado, and P. F. O'Mahony
Department of Mathematics, Royal Holloway, University of London, Egham, Surrey TW20 0EX, United Kingdom
(Received 11 June 1998)

We analyze the influence of classical phase-space structures on the ionization behavior of Rydberg atoms in parallel electric and magnetic fields. Classically, ionization above the Stark saddle-point energy is suppressed for moderate magnetic fields compared to zero magnetic field. The location of a stable periodic orbit in the surface of section serves as a criterion to understand this trend. For strong magnetic fields the effect is reversed, and ionization is enhanced. This fact is related to the onset of global chaos in the Hamiltonian system. We provide an analytic criterion for the field values at which this crossover takes place. [S1050-2947(98)04011-6]

PACS number(s): 32.80.Rm, 32.60.+i, 05.45.+b

I. INTRODUCTION

Rydberg atoms in static external fields have attracted much interest over recent years, since they belong to the most basic quantum systems exhibiting chaos which nevertheless are experimentally realizable [1]. They are therefore ideally suited to study the fundamental question as to how classically chaotic behavior in Hamiltonian systems is reflected in their quantum-mechanical counterparts (''quantum chaology'') [2]. To date most of the experiments and theoretical calculations have focused on explaining the long-range modulations seen in photoabsorption spectra of Rydberg atoms in magnetic or combined electric and magnetic fields. An elaborate semiclassical theory has been developed, which relates these modulations to the closed orbits of the corresponding classical system, starting from the nucleus and returning back to it (''closed-orbit theory'') [3–6]. In contrast, relatively few investigations have addressed the question as to how Rydberg electrons ionize, once they have been laser excited, in the presence of external fields. In the time domain the ionization dynamics of laser-excited Rydberg wave packets subject to an additional homogenous electric field has been studied theoretically [7] and experimentally [8].

In this paper we study ionization of highly excited Rydberg electrons in parallel electric and magnetic fields in the frequency regime, that is at fixed energy. The addition of a magnetic field introduces a feature into the phase space of the corresponding classical Hamiltonian which is not present in a pure electric field: If potentials of competing symmetry exercise an equally strong influence on the electron its motion may become chaotic. This prompts the question as to what is the influence of the classically chaotic dynamics on the ionization behavior of the Rydberg electron. We describe ionization within a classical framework, aiming to understand the trends in the ionization behavior in terms of the classical phase-space structure. A semiclassical or even quantum-mechanical theory for field ionization in external fields is still out of reach due to the spacially extended nature of the wave functions involved.

Our investigations have also been motivated by a recent experiment on Rydberg atoms in crossed electric and magnetic fields [9]. This type of experiment is able to distinguish between stable and ionizing states above the classical field ionization threshold on a microsecond time scale $T_{\max} \approx 20\ \mu$s. It thus differs from the above-mentioned photoexcitation experiments in external fields for which closed-orbit theory can be applied. Quantum mechanically, this experiment measures the ratio of photoexcited states with a decay width larger than $\Gamma = 2\pi/T_{\max}$ to the total density of photoexcited states at the excitation energy. A nonmonotonic progression of the ionization threshold in crossed fields, defined as the energy above which the percentage of ionized atoms to the total number of photoexcited atoms is larger than 50%, was observed as the magnetic field was changed. This ionization behavior was shown to depend only on the scaled parameters of the corresponding classical system (see below), and a subsequent theoretical interpretation based on classical trajectory calculations confirmed the behavior found by the experiment [10].

The plan of the paper is as follows: We briefly review the classical description of a Rydberg electron in parallel electric and magnetic fields in Sec. II. In Sec. III, we present the global ionization behavior as a function of the field parameters and the energy. The relationship to parameter ranges in typical experiments is briefly discussed. In Sec. IV we explain the trends of the ionization probability as a function of the field parameters and the energy in terms of the classical phase-space structure. We show that the overall behavior of the ionization cross section can be related to the appearance of two periodic orbits of the Hamiltonian: (a) For small and intermediate magnetic fields, the so-called downhill balloon orbit creates an island of stability which takes flux away from the ionization channel, and (b) for large magnetic fields an unstable periodic orbit is created which leads to an enhancement of the ionization probability. An analytic criterion is derived giving the field values at which this crossover occurs. Finally, in Sec. V, we discuss the relationship between the results presented here and closed-orbit theory. We also address the question as to how a nonhydrogenic core influences the ionization behavior. More technical aspects are left to the Appendix.

An experimental test of the results presented here is yet outstanding, but could be performed along the same lines as has been done for the crossed-field experiment. Atomic units will be used throughout the paper unless otherwise stated.

 ©1998 The American Physical Society

II. HYDROGEN IN PARALLEL ELECTRIC AND MAGNETIC FIELDS

The Hamiltonian for a hydrogen atom in a homogeneous electric field F and a parallel magnetic field B, both oriented parallel to the z axis, in a reference frame rotating with the Larmor frequency, is

$$H=\frac{\mathbf{p}^2}{2}-\frac{1}{r}+\frac{B^2}{8}(x^2+y^2)-Fz. \tag{1}$$

B and F are measured in atomic units ($B_0=2.35\times10^5$ T, $F_0=5.14\times10^9$ V cm^{-1}). Introducing scaling relations for the coordinates, the momenta, the Hamiltonian, and the time as $\mathbf{r}\rightarrow B^{-2/3}\mathbf{r}$, $\mathbf{p}\rightarrow B^{1/3}\mathbf{p}$, $H\rightarrow B^{2/3}H$ and $t\rightarrow t/B$, the scaled Hamiltonian function reads

$$H_{\rm sc}=\frac{\mathbf{p}^2}{2}-\frac{1}{r}+\frac{1}{8}(x^2+y^2)-fz, \tag{2}$$

where $f=B^{-4/3}F$ is the scaled electric field. The scaling property of the Hamiltonian function means that the classical dynamics does not depend on the three parameters B, F, and energy E independently, but only on the scaled electric field f and the scaled energy $\varepsilon=B^{-2/3}E$. The scaled Hamiltonian (2) is the starting point for our analysis of ionization in parallel electric and magnetic fields. In the rest of the paper, $\mathbf{r}$ and $\mathbf{p}$ denote scaled quantities unless otherwise stated. Note that for a fixed electric field F, the scaled electric field f decreases with increasing magnetic field B. The z component of the angular momentum L_z or its scaled counterpart $l_z=B^{1/3}L_z$ are conserved quantities. We will confine ourselves to the case where the $l_z=0$ manifold is excited. Due to the cylindrical symmetry l_z is a conserved quantity and the phase space of the parallel field Hamiltonian (2) is effectively four dimensional.

III. IONIZATION AND PHASE-SPACE STRUCTURE

A. Ionization probabilities

Photoexcitation takes place from a low-lying state which is well localized within a few Bohr radii from the nucleus. For a high-lying state to be laser excited, it must have considerable overlap with the low-lying state. Neglecting tunneling effects, the wave function of the excited state can be constructed semiclassically according to Huygens principle [11] from outgoing Coulomb waves [3]. The characteristics of wave fronts are classical trajectories starting at the origin $r=0$.

Trajectories in parallel electric and magnetic fields ionize in the direction of the positive-z axis, since the diamagnetic term in Eq. (2) acts as a confining potential in the other coordinates. The sum of all static potentials has a local maximum at the Stark saddle $x_s=y_s=0$ and $z_s=1/\sqrt{f}$. Classically the threshold for ionization is the Stark saddle-point energy $\varepsilon_s=-2\sqrt{f}$.

In numerical simulations trajectories were started at the origin $r=0$ within a one-dimensional initial manifold characterized by the azimuthal angle $\theta\in[0,\pi]$ with respect to the z axis. The equations of motion were then solved by writing the scaled Hamiltonian (2) in semiparabolic coordinates as described in the Appendix. This removes the Coulomb singularity at the origin (see also Ref. [12]). A high-order Taylor integrator was used as described in Ref. [13], which reduced computation times by a factor of approximately 3 compared to conventional Runge-Kutta methods. Trajectories were propagated from the origin $r=0$ until the time $T_{\rm max}=250T_K$, where $T_K=2\pi/(-2\varepsilon)^{3/2}$ is the Kepler time (in scaled units) for the electron motion in zero external fields. A trajectory is recorded as ionized if the condition $z>2z_s$ is fulfilled within $t\leqslant T_{\rm max}$.

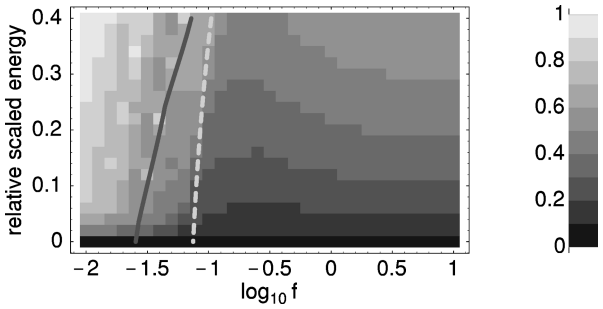

FIG. 1. Classical ionization probability (ratio of ionizing trajectories) on a 2D grid of the scaled electric field f in atomic units, and the dimensionless scaled energy $\varepsilon_r=1-\varepsilon/\varepsilon_s$ relative to the classical ionization threshold ε_s. The right panel gives the coding of the ratio of ionizing trajectories. Light shaded areas indicate a high ionization probability. Dashed line: bifurcation of the almost circular orbit [+] [Eq. (11)]. Along the solid line the Kepler frequency ω_K and the Larmor frequency $\omega_L^{(+)}$ are equal [see the discussion after Eq. (6)].

In Fig. 1, we present the global picture of the ionization probability as a function of the scaled electric field and the scaled energy. Light shaded areas indicate values of the scaled parameters with a high ionization probability, and dark shaded areas belong to values of f and ε where only a small ratio of trajectories ionize. The energy $\varepsilon_r=1-\varepsilon/\varepsilon_s$ is plotted relative to the Stark energy. The scaled electric field is plotted on a logarithmic scale, and varies over three orders of magnitude. If the scaled energy ε_r relative to the energy of the Stark saddle point is kept fixed, and the scaled electric field is decreased (going from right to left in Fig. 1) the ionization probability decreases first. However, below approximately $\log_{10} f=-1.1$ the trend is reversed, and ionization is enhanced again. In Fig. 2 we have plotted a cut through the ionization probabilities of Fig. 1 taken at constant relative scaled energies $\varepsilon_r=0.1$ a.u. and $\varepsilon_r=0.2$ a.u. The rise in the ionization probability for small scaled electric fields or large magnetic fields, respectively, is clearly visible.

We briefly discuss the connection between the scaled parameters depicted in Fig. 2 and typical field strengths used in laboratory experiments. In the crossed-field experiments [9] the electric-field strength was kept fixed and the magnetic-field strength changed. A typical electric-field strength used was $F=30$ V/cm. The highest scaled electric field $f=10$ a.u. in Fig. 2 then corresponds to a magnetic field of $B=0.028$ T, and the lowest scaled electric field $f=0.01$ a.u. corresponds to $B=4.96$ T. Keeping the electric field fixed has the advantage that a fixed relative scaled energy ε_r is equivalent to a fixed unscaled excitation energy E of the Rydberg atom. In an experiment which measures the ionization flux at constant ε_r, the laser frequency can then

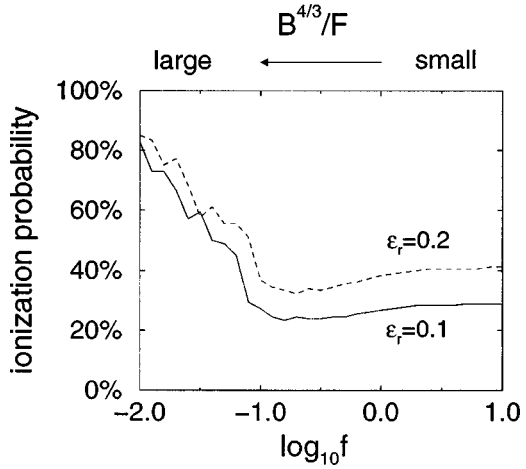

FIG. 2. Classical ionization probability at two fixed relative scaled energies $\varepsilon_r=0.1$ and $\varepsilon_r=0.2$ (dimensionless) as a function of the scaled electric field f in atomic units. For a fixed unscaled electric field F, the magnetic field B increases going from right to left in the figure.

be kept fixed. The Stark saddle-point energy $\varepsilon_s=-2\sqrt{f}$ for the above field parameters corresponds to the excitation of the principal quantum number $n\approx 57$ (if no external fields were present). The relative scaled energies $\varepsilon_r=0.1$ a.u. and $\varepsilon=0.2$ a.u. correspond to $n\approx 69$ and 74, respectively, which is accessible in present day experiments.

B. Ionization times

To gain a better understanding of the nonmonotonic behavior of the ionization probability, as depicted in Fig. 2, the ionization time as a function of the starting angle θ is plotted in Figs. 3(a)–3(d) for four different parameter regimes of the scaled electric field f. The relative scaled energy is kept fixed at $\varepsilon_r=0.125$. For a strong scaled electric field ($f=1.44$), trajectories which start within a cone $\theta<0.3\pi$, whose axis points towards the Stark saddle point, ionize on a fast time scale [Fig. 3(a)]. If the scaled electric field is decreased ($f=0.36$) a second interval of starting angles, centered around $\theta=0.27\pi$ appears in addition to the one of Fig. 3(a), for which trajectories do not ionize [Fig. 3(b)]. For an even smaller scaled electric field ($f=0.1225$), the ionization time becomes a highly irregular function of the starting angle θ in the interval $\theta\in[0.18\pi,0.33\pi]$ [Fig. 3(c)]. Finally, and most importantly, in the regime of weak scaled electric field ($f=0.04$), trajectories starting toward the uphill side of the electric field in an interval $\theta\in[0.71\pi,0.89\pi]$ are able to ionize within the time $T_{\max}$ [Fig. 3(d)]. Thus, classically, ionization is enhanced in the regime of a small scaled electric field due to the opening of an ionization channel which is not present at low or intermediate magnetic fields. Ionization via this channel takes place on a much longer time scale than the fast, direct ionization in the cone around the downhill axis of the potential ($\theta=0$), and the ionization time is an irregular function of the starting angle. A fractal structure of classical ionization times as a function of initial conditions has previously been found for hydrogen in crossed electric and magnetic fields [14]. Such a structure is a signature of chaotic motion in phase space, as we will show in detail in Sec. III C.

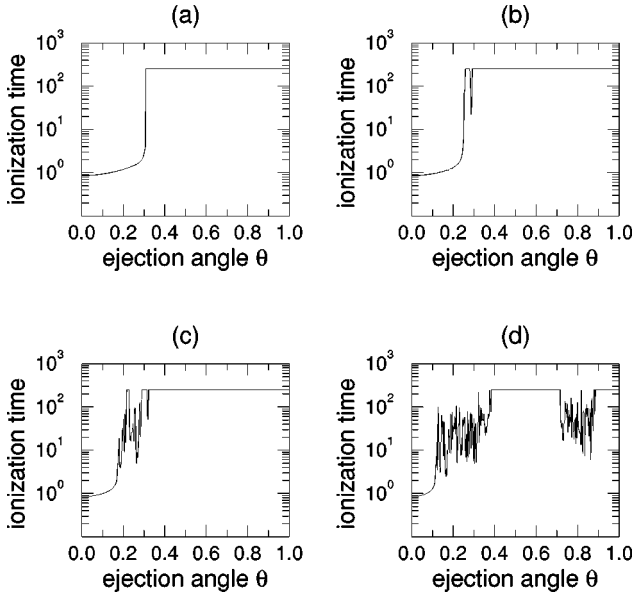

FIG. 3. Ionization time in units of the Kepler time $T_K=2\pi/(-2\varepsilon)^{3/2}$ of the field-free motion as a function of the azimuthal starting angle θ with respect to the z axis. Scaled electric fields in atomic units from (a)–(d): $f=1.44$, 0.36, 0.1225, and 0.04. The dimensionless relative scaled energy is $\varepsilon_r=0.125$ in all cases.

C. Phase-space structure

To interpret the ionization behavior in the different parameter regimes in terms of the classical phase space structure we created Poincaré surface of section (PSOS) plots using the scaled Hamiltonian (2). We plotted PSOS's in the pair of action-angle variables $(a_z\sqrt{-2\varepsilon},\phi_{a_z})$ introduced in the Appendix. The use of these variables has the advantage that the connection to results in the perturbative regime (see Sec. IV B) is easily made. The action variable $a_z\sqrt{-2\epsilon}$ is proportional to the z component of the modified Runge-Lenz vector (in unscaled variables) [15,16]

$$\mathbf{A}=\frac{1}{\sqrt{-2H_0}}\left(\mathbf{p}\times\mathbf{L}-\frac{\mathbf{r}}{r}\right), \tag{3}$$

which is a conserved quantity in first-order perturbation theory in the external fields. H_0 is the part of the Hamiltonian (1) which is independent of the external fields:

$$H_0=\frac{\mathbf{p}^2}{2}-\frac{1}{r}. \tag{4}$$

Second, at the nucleus $r=0$ the full Hamiltonian (1) and its field-independent part (4) coincide; therefore $E=H_0$, and the exact relationship

$$a_z\sqrt{-2\varepsilon}=-\cos\,\theta \tag{5}$$

between the azimuthal starting angle θ of trajectories and the action variable a_z holds. From the transformation formulas of the Appendix one can derive that the conjugate angle variable has the value $\phi_{a_z}=\pm\pi/2$ at the origin $r=0$.

Figure 4 translates the ionization time results into PSOS's. Surface of sections were taken whenever a trajectory crossed the z axis. In strong scaled electric fields and for

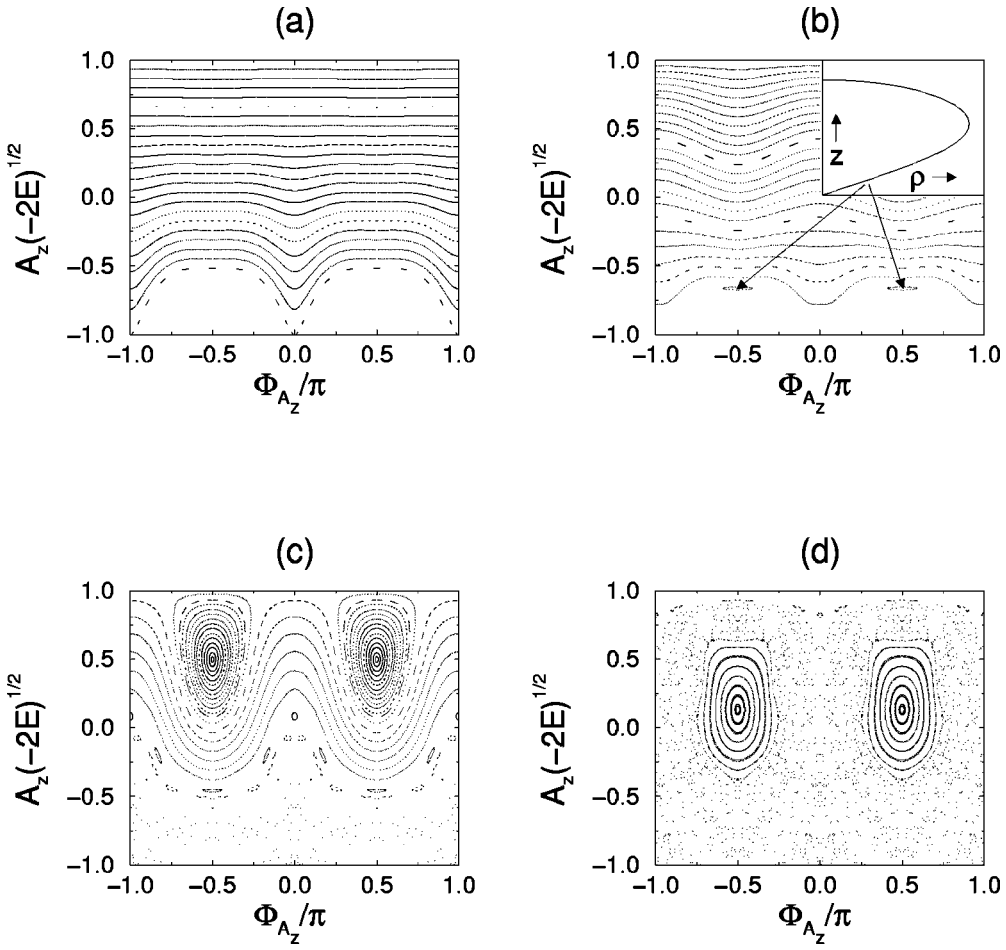

FIG. 4. Surface of sections at $\rho=\sqrt{x^2+y^2}=0$ in the pair of coordinates $(\phi_{a_z}/\pi, a_z\sqrt{-2\varepsilon})$ (all quantities in atomic units). The scaled electric field and the scaled energy are the same as in Figs. 3(a)–3(d). The inset in (b) shows one-half of the downhill balloon orbit in (ρ,z) coordinates with the origin in the lower left corner. (The other half is obtained by reflection on the z axis.) The arrows indicate the position of this orbit in the surface of section.

trajectories which start toward the uphill side of the electric field potential, $a_z\sqrt{-2\varepsilon}$ is an almost conserved quantity [Fig. 4(a)]. This is related to the fact that the Runge-Lenz vector is a conserved quantity for the first-order Stark effect. The starting condition $r=0$ corresponds to the lines $\phi_{a_z}=\pm\pi/2$ in the surface-of-section plots. The relation between the starting angle θ and $a_z\sqrt{-2\varepsilon}$ is given by Eq. (5). The fast ionizing trajectories starting toward the downhill side lead to the white area in the PSOS's in the interval $a_z\sqrt{-2\varepsilon}\in[-1.0,-0.6]$. In Fig. 4(b), a small island shows up around $a_z\sqrt{-2\varepsilon}=-0.667$. It belongs to a stable orbit, the so-called downhill balloon orbit, named $[0-]$ in the classification scheme of periodic orbits of Eckhardt and Wintgen [17] (see also Ref. [18]). The downhill balloon orbit is shown in the inset of Fig. 4(b). The arrows indicate the location of the island of stability of this orbit. The island created by the downhill balloon orbit is responsible for the reduction of the percentage of ionizing trajectories in the parameter regime of Fig. 4(b). We will come back to this point in detail in Sec. IV A. For a smaller scaled electric field [Fig. 4(c)], chaotic ionization can be seen in the lower part of the figure. The other main feature compared with Fig. 4(b) is the existence of a stable periodic orbit at $\phi_{a_z}=\pm 0.5\pi$, where $a_z\sqrt{-2\varepsilon}\approx 0.5$. This is the so-called [0] orbit which for pure magnetic fields lies in the plane perpendicular to the magnetic field. In the presence of an electric field its starting angle is shifted toward the uphill side of the electric-field potential [19]. Finally in Fig. 4(d), for a small scaled electric field or a high magnetic field, most of the phase space is chaotic with the exception of the stable island around the [0] orbit. Chaotic ionization can now also proceed for trajectories with initially positive a_z. Due to this possibility ionization is enhanced.

IV. DIFFERENT IONIZATION REGIMES

A. Regime of suppressed ionization

In this section we explain the behavior of the ionization cross section for intermediate and large scaled electric fields ($\log_{10} f > -1.1$). Close inspection of the PSOS plots for different values of f and ε revealed that the stable island associated with the above mentioned downhill balloon orbit $[0-]$ is always very closely situated near the last remnant Kolmogorov-Arnold-Moser (KAM) torus with the topology of the pure Stark problem which reaches from $\phi_{a_z}=-\pi$ to $\phi_{a_z}=\pi$ [see Fig. 4(b)]. Although the downhill balloon orbit together with its surrounding stable island does not ionize itself its location in the PSOS plots indicates the cone of

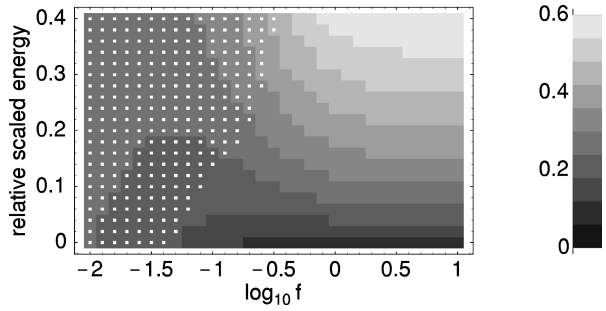

FIG. 5. Starting angle θ_0 of the downhill balloon orbit $[0-]$. Axes and units are as in Fig. 1. The right panel gives the darkness coding of θ_0/π. Dark shaded areas indicate a small starting angle θ_0 with respect to the z axis. The white dots indicate the region where the $[0-]$ orbit is unstable.

angles within which trajectories must start to be able to ionize in the regime of strong and intermediate scaled electric fields.

Figure 5 shows the starting angle θ_0 of the downhill balloon orbit, determined numerically, as a function of the scaled electric field and the scaled energy. Dark coded areas indicate a small starting angle with respect to the axis of the external fields, and light coded areas a large angle. The downhill balloon orbit is unstable in the region indicated by the white dots. In the region, where it is stable, Fig. 5 closely resembles the behavior of Fig. 1. Thus for strong and intermediate scaled electric fields, or low and intermediate magnetic fields B compared to the electric field F, the suppression of the ionization probability can be directly related to the starting angle θ_0 of a single *bound periodic* orbit. The argument is valid in the regime where the downhill balloon orbit is stable, and thus creates an island which takes away flux from the downhill ionization channel.

B. Regime of enhanced ionization

In this section we derive an analytic criterion for the crossover border between suppressed ionization for intermediate magnetic fields and enhanced ionization at strong magnetic fields. To do this we will use results from classical perturbation theory for hydrogen in parallel electric and magnetic fields. The scaled Hamiltonian (2), expressed in the action-angle variables of the unperturbed Kepler problem (see the Appendix), can be averaged over one period of the fast motion, which is the motion along the perturbed Kepler ellipse. This leads to an adiabatic Hamiltonian [15,16,20], for which the scaled action n_{sc} is a constant of motion. A second—adiabatic—invariant exists [10,15], which (expressed in scaled quantities) reads as

$$\Lambda = -2(n_{sc}^2 - a_z^2)\cos(2\phi_{a_z}) + 2n_{sc}^2 - 3a_z^2 + \frac{24f}{n_{sc}}a_z + 3f^2 n_{sc}^2 a_z^2 . \quad (6)$$

The use of perturbation theory is justified as long as the scaled Kepler frequency $\omega_K = 1/n_{sc}^3$ of the unperturbed motion over which the perturbed motion is averaged is much larger than the two Larmor type frequencies $\omega_L^{(\pm)} = 2^{-1}|1 \pm 3n_{sc}f|$ introduced by the external fields [10]. The condition $\omega_K > \omega_L^{(+)}$ is fulfilled to the right of the solid line in Fig. 1.

To make the connection to trajectories starting at the origin, one notices that $\varepsilon = -1/(2n_{sc}^2)$ is an exact relation for trajectories when they pass the nucleus, $r=0$. The crucial point in the argument now is that this relation still holds approximately in the perturbative regime for the dynamics not too far away from the nucleus, and we therefore replace

$$n_{sc} \to 1/\sqrt{-2\varepsilon} \quad (7)$$

in Eq. (6). To simplify formulas the additional rescaling $a_z = n_{sc}\tilde{a}_z$ and $\Lambda = n_{sc}^2\tilde{\Lambda}$ is performed. In terms of ε and f the adiabatic invariant is then approximately

$$\tilde{\Lambda} = -2(1-\tilde{a}_z^2)\cos(2\phi_{a_z}) + 2 + 10\beta\tilde{a}_z + 2\gamma\tilde{a}_z^2 , \quad (8)$$

where we have introduced

$$\beta = 24f|\varepsilon|/5, \quad \gamma = -\tfrac{3}{2}[1 - f^2/(2|\varepsilon|)] \quad (9)$$

in accordance with previous notation [16]. The key to explaining the opening of the ionization channel for orbits starting toward the uphill side of the potential is to relate it to the creation of an unstable periodic orbit, the so-called almost circular or $[+]$ orbit at certain combinations of f and ε. The $[+]$ orbit does *not* go through the origin. It nevertheless influences the ionization behavior drastically due to the creation of a separatrix along which uphill orbits can diffuse and finally ionize. The $[+]$ orbit is an unstable fixed point in the PSOS. Perturbatively it can be calculated from the condition $\partial\tilde{\Lambda}/\partial\phi_{a_z} = \partial\tilde{\Lambda}/\partial\tilde{a}_z = 0$ as a critical point of the equipotential lines of the adiabatic invariant (8). It is located at

$$\phi_{a_z} = 0, \quad \tilde{a}_z = -5\beta/[2(1+\gamma)]. \quad (10)$$

The orbit exists when $|\tilde{a}_z| \leqslant 1$, which is fulfilled when the scaled parameters obey the relation

$$\frac{5\beta}{2} \leqslant |1+\gamma|. \quad (11)$$

For the $[+]$ orbit to be unstable the critical point must be a saddle point which is the case when $\gamma > -1$. In the range of the scaled field parameters in Fig. 1 the $[+]$ orbit is always unstable if it exists and the values of f and ε at which it is created are given by Eq. (11), and are plotted as the white dashed line in Fig. 1. The almost circular orbit exists left of this line giving rise to the uphill ionization channel. Condition (11) predicts the onset of enhanced ionization very accurately.

Note that because of the conservation of n_{sc}, the perturbative Hamiltonian has a bound phase space, whereas we wish to analyze the onset of chaotic ionization for the unbound motion of the full Hamiltonian (2). However, in the region close to the nucleus the external fields are small compared to the Coulomb potential, and the perturbative treatment is always valid. The argument then is that *if* the ionization dynamics is influenced by the phase-space structure near the nucleus, the perturbative Hamiltonian can be employed.

Classical chaotic ionization is a necessary condition for the occurrence of Ericson fluctuations [21] in a quantum spectrum due to broad overlapping resonances. This fact has

been demonstrated for hydrogen in crossed electric and magnetic fields [14]. The above criterion [Eq. (11)] therefore also provides a guideline for the parameter regimes in photoexcitation experiments in parallel electric and magnetic fields where the manifestions of the classically chaotic dynamics in the form of Ericson fluctuations could be tested.

V. DISCUSSION

In the classical description of ionization, presented here, an electron leaves the region near the nucleus on a trajectory which can either ionize or remain bound in phase space. The ionization probability is the ratio of ionizing trajectories to the total number of trajectories on the initial manifold in phase space. We can relate such a description of ionization to the semiclassical closed-orbit theory of photoexcitation [3–5]. It is important to recognize that closed-orbit theory itself cannot make any predictions about the *stability* of a manifold of excited states against ionization.

In closed-orbit theory an initial outgoing Coulomb wave, produced by photoexcitation, is responsible for the direct or background part of the photoabsorption cross section. At distances of approximately 50-bohr radii the outgoing wave is continued semiclassically. Only bound trajectories contribute to this construction and among them those which return to the nucleus play a prominent role in closed-orbit theory. The returning trajectories are continued by incoming Coulomb waves in the region near the nucleus. Interference between outgoing and incoming waves leads to oscillations in the absorption spectrum as a function of the excitation energy. This picture also remains valid in the context of field ionization. As for the photoabsorption spectrum, it is expected that in a fully semiclassical description the interference between the outgoing wave and incoming waves gives rise to oscillations in the ionization probability as a function of the scaled energy. However, carrying out a fully semiclassical description of ionization in a consistent manner would, first of all, require one to construct a semiclassical S matrix [22], which incorporates phases and amplitudes of the ionizing trajectories, which we discussed in Sec. III. At least in the chaotic regime, which is the most interesting, such a semiclassical construction of the S matrix seems extremely difficult if not intractable because of the fractal structure of the time delay function (see Fig. 3). The classical description of ionization therefore predicts the direct or smooth part of the ionization rate, neglecting interference effects due to closed trajectories.

Core scattering of Rydberg electrons induces additional modulations in the photoexcitation spectra of nonhydrogenic Rydberg atoms which are not present in hydrogen [23,24]. However, since the classical theory of ionization is insensitive to such modulations, our results for the background ionization probability should also apply to nonhydrogenic atoms like lithium or rubidium. The success of classical trajectory calculations in the hydrogenic approximation in reproducing the ionization behavior for rubidium atoms in crossed electric fields [10] also supports this argument.

The ionization behavior was calculated in Sec. III A, assuming an equal distribution of starting trajectories in the azimuthal angle θ. More accurately the dependence of the probability distribution of starting angles on the angular momentum character of the initial state and the laser polarization must be taken into account. Work on incorporating the effects of laser polarization and the initial state from which laser excitation takes place is in progress.

A final question which needs to be addressed is whether the classical enhancement of ionization due to the chaotic ionization dynamics can survive quantum-mechanically. It has been demonstrated for the problem of microwave ionization of atoms that quantum-mechanical coherence effects, that is interference between ionization trajectories, can suppress the effects of classically chaotic dynamics [25], a phenomenon known as dynamical localization. It would therefore be very interesting to test experimentally whether the chaotically enhanced ionization at relatively small scaled electric fields, predicted on classical grounds, can indeed be observed.

VI. SUMMARY

In summary, we predict the ionization behavior of Rydberg atoms in parallel electric and magnetic fields over a wide range of field parameters on the basis of the classical phase-space structure. At a fixed energy relative to the Stark energy, the ionization probability varies nonmonotonically as the scaled electric field is changed. We have related this behavior to two periodic orbits in the system. The stability island created by the downhill balloon orbit was identified to be responsible for the suppression of ionization for intermediate scaled electric fields compared to the case of a pure electric field. For small scaled electric fields, or a strong magnetic field compared to the electric field, a crossover to enhanced, chaotic ionization takes place. An analytic criterion for this crossover based on the creation of the unstable almost circular orbit was derived. We thus demonstrated that the ionization behavior in an unbound Hamiltonian system can be related to bound periodic orbits of this system.

ACKNOWLEDGMENTS

It is a pleasure to thank A. Buchleitner, H. Held, G. Raithel, H. Walther, and T. Uzer for stimulating discussions. W. I. gratefully acknowledges financial support from the EU Marie Curie scheme under the Training and Mobility of Researchers Programme. We also acknowledge financial support from the EU Human Capital and Mobility program.

APPENDIX: HAMILTONIAN IN ACTION-ANGLE VARIABLES

The singularity of the scaled Hamiltonian (2) can be removed if semiparabolic coordinates (u,v) are introduced:

$$\rho=\sqrt{x^2+y^2}=uv, \quad z=\tfrac{1}{2}(u^2-v^2). \tag{A1}$$

Additionally the new timelike variable s is defined via

$$dt=(u^2+v^2)ds. \tag{A2}$$

The regularized Hamiltonian function reads

$$\mathcal{H}\equiv 2=\frac{1}{2}(p_u^2+p_v^2)-\varepsilon(u^2+v^2)+\frac{1}{8}u^2v^2(u^2+v^2)$$
$$-\frac{f}{2}(u^4-v^4). \tag{A3}$$

The Hamiltonian can then be expressed in terms of action-angle variables of the unperturbed Kepler problem by performing a succession of three canonical transformations. In the first step new pairs of conjugate variables (q_1,p_1) and (q_2,p_2) are introduced:

$$\begin{aligned} u&=(-2\varepsilon)^{-1/4}(q_1+p_1), \quad p_u=(-2\varepsilon)^{1/4}(q_1-p_1),\\ v&=(-2\varepsilon)^{-1/4}(q_2+p_2), \quad p_v=(-2\varepsilon)^{1/4}(q_2-p_2). \end{aligned} \tag{A4}$$

The transformation to action-angle variables (I_i,ϕ_i) is achieved by

$$q_i=\sqrt{2I_i}\sin\,\phi_i, \quad p_i=\sqrt{2I_i}\cos\,\phi_i \quad (i=1,2). \tag{A5}$$

A final transformation relates these variables to the action-angle variables of the unperturbed Kepler problem (for $l_z=0$):

$$\begin{aligned} I_1&=\tfrac{1}{2}(n_{\rm sc}+a_z), \quad \phi_1=\phi_{n_{\rm sc}}+\phi_{a_z}\\ I_2&=\tfrac{1}{2}(n_{\rm sc}-a_z), \quad \phi_2=\phi_{n_{\rm sc}}-\phi_{a_z}. \end{aligned} \tag{A6}$$

The scaled action variables $n_{\rm sc}$ and a_z are related to their unscaled counterparts used in Ref. [15] via $n_{\rm sc}=B^{1/3}n$ and $a_z=B^{1/3}A_z$, where A_z is the z component of the unscaled modified Runge-Lenz vector equation (3).

[1] For a comprehensive bibliography of experimental and theoretical work on atoms in external fields, see C. Neumann, R. Ubert, S. Freund, E. Flöthmann, B. Sheehy, K. H. Welge, M. R. Haggerty, and J. B. Delos, Phys. Rev. Lett. **78**, 4705 (1997).

[2] *Quantum Chaos: Between Order and Disorder*, edited by G. Casati and B. Chirikov (Cambridge University Press, Cambridge, 1995).

[3] M. L. Du and J. B. Delos, Phys. Rev. A **38**, 1896 (1988); **38**, 1913 (1988).

[4] J. Gao and J. B. Delos, Phys. Rev. A **46**, 1455 (1992).

[5] J.-M. Mao, K. A. Rapelje, S. J. Blodgett-Ford, J. B. Delos, A. König, and H. Rinneberg, Phys. Rev. A **48**, 2117 (1993).

[6] M. Courtney, Phys. Rev. A **51**, 4558 (1995).

[7] F. Robicheaux and J. Shaw, Phys. Rev. Lett. **77**, 4154 (1996); Phys. Rev. A **56**, 278 (1997).

[8] G. M. Lankhuijzen and L. D. Noordam, Phys. Rev. A **52**, 2016 (1995); Phys. Rev. Lett. **76**, 1784 (1996).

[9] G. Raithel and H. Walther, Phys. Rev. A **49**, 1646 (1994).

[10] J. von Milczewski, D. Farrelly, and T. Uzer, Phys. Rev. A **56**, 657 (1997).

[11] J. B. Delos, Adv. Chem. Phys. **65**, 161 (1986).

[12] E. L. Stiefel and G. Scheifele, *Linear and Regular Celestial Mechanics* (Springer-Verlag, Berlin, 1971).

[13] H. D. Meyer, J. Chem. Phys. **84**, 3147 (1986).

[14] J. Main and G. Wunner, Phys. Rev. Lett. **69**, 586 (1992); J. Phys. B **27**, 2835 (1994).

[15] D. Farrelly, T. Uzer, P. E. Raines, J. P. Skelton, and J. A. Milligan, Phys. Rev. A **45**, 4738 (1992).

[16] J. von Milczewski and T. Uzer, Phys. Rev. A **56**, 220 (1997).

[17] B. Eckhardt and D. Wintgen, J. Phys. B **23**, 355 (1990).

[18] W. Schweizer, *Das diamagnetische Wasserstoffatom: ein Beispiel für Chaos in der Quantenmechanik* (Verlag Harri Deutsch, Frankfurt, 1995).

[19] S. Bivona, W. Schweizer, P. F. O'Mahony, and K. T. Taylor, J. Phys. B **21**, L671 (1988).

[20] T. P. Grozdanov and M. J. Raković, J. Phys. B **23**, 3531 (1990).

[21] R. Blümel and U. Smilansky, Phys. Rev. Lett. **60**, 477 (1988).

[22] W. H. Miller, Adv. Chem. Phys. **25**, 69 (1974).

[23] B. Hüpper, J. Main, and G. Wunner, Phys. Rev. A **53**, 744 (1996).

[24] P. A. Dando, T. S. Monteiro, D. Delande, and K. T. Taylor, Phys. Rev. A **54**, 127 (1996).

[25] F. Benvenuto, G. Casati, and D. L. Shepelyansky, Phys. Rev. A **55**, 1732 (1997).